Compact X-Ray Tube With Ceramic Vacuum Seal for Portable and Robust Dental Imaging

Amar Prasad Gupta, Jinho Choi, Mallory Mativenga, *Member, IEEE*, Keunhwa Park, Jaekyu Jang, Seung Jun Yeo, Jaeik Jung, Moon Shik Chae, Byeong-No Lee, Jejin Jang, He-Lin Zhu, Hyung-Soo Mok, Jeung Sun Ahn, and Jehwang Ryu

***Abstract*— A major challenge for glass X-ray tube makers is the reduction in the tube size for portable or handheld applications. Size reduction is difficult mainly due to contact size restrictions for glass-to-metal welding. In high-voltage (60–70 kV) portable applications such as dental imaging, a distance of at least 5 mm should be maintained between the anode and the glass envelope to prevent the latter from burnout, which further limits reduction in the tube's diameter. In this study, reduction in the size of a dental X-ray tube by approximately 43% is achieved by replacing the glass envelope with ceramic. Instead of welding, the ceramic body permits the use of brazing, which supports extremely small contact sizes. Additionally, due to the higher dielectric constant of ceramic, even less than 1 mm spacing is permissible between the envelope and the anode, enabling further size reduction. Despite the 43% reduction in size, limiting spatial resolutions of approximately 8 and 7 lines per mm are obtained for the ceramic and glass sealed tubes, respectively. Moreover, the two tubes obtain similar X-ray images of human teeth, verifying the potential of the compact-size ceramic X-ray tube in dental imaging.**

***Index Terms*— Brazing, ceramic, dental, filament, X-ray.**

Manuscript received May 25, 2021; revised July 5, 2021; accepted July 12, 2021. This work was supported in part by the Bio and Medical Technology Development Program of the National Research Foundation (NRF) funded by the Ministry of Science and ICT under Grant NRF-2018M3A9E9024942 and Grant NRF-2016M3A9E9942010, in part by the National Research Council of Science and Technology (NST) grant by the Korea Government under Grant CAP-18-03-ETRI and Grant 1711077860, and in part by the Ministry of Small and Medium Enterprises (SMEs) and Startups Korea under Grant 1425151329. The review of this article was arranged by Editor R. Letizia. *(Corresponding authors: Jehwang Ryu; Mallory Mativenga.)*

Amar Prasad Gupta and Jeung Sun Ahn are with the Department of Physics, Kyung Hee University, Seoul 02447, South Korea.

Jinho Choi is with the Department of Radiation Oncology, College of Medicine, Kyung Hee University, Seoul 02447, South Korea.

Mallory Mativenga is with the Department of Information Display, Kyung Hee University, Seoul 02447, South Korea (e-mail: mallory@khu.ac.kr).

Keunhwa Park and Jehwang Ryu are with the Department of Radiology, College of Medicine, Kyung Hee University, Seoul 02447, South Korea (e-mail: jhryu@khu.ac.kr).

Jaekyu Jang, Seung Jun Yeo, and Jaeik Jung are with CAT Beam Tech. Company Ltd., Seoul 02455, South Korea.

Moon Shik Chae and Byeong-No Lee are with the Korea Atomic Energy Research Institute, Jeollabuk-do 56212, South Korea.

Jejin Jang, He-Lin Zhu, and Hyung-Soo Mok are with the Department of Electrical and Engineering, Konkuk University, Seoul 05029, South Korea.

Color versions of one or more figures in this article are available at https://doi.org/10.1109/TED.2021.3097315.

Digital Object Identifier 10.1109/TED.2021.3097315

I. Introduction

FOR more than a century, X-ray tubes have been known to consist of a vacuum-sealed glass tube containing a filament-based electron source (the cathode) and an electron-absorbing anode [1], [2]. The filament is typically a tungsten coil, which creates free electrons through thermionic emission [3]. Electrons from the cathode collide with the anode material, usually molybdenum, tungsten, or copper. Upon collision, some of the energy of the electrons from the cathode is transferred to the electrons within the anode material, thereby exciting them to higher energy levels [4]. A small amount of the energy generated (about 1%) is emitted as X-rays when these excited electrons fall back to lower energy levels inside the anode material [5].

The glass tube is important as it creates an air-free vacuum around the cathode and anode to prevent the scattering of electrons by air particles and protects the anode and cathode from oxidation and corrosion [6]. However, the use of glass as the envelope for X-ray tubes has its limitations. The most notable limitation is that glass-to-metal welding is restricted to contact sizes not less than a few millimeters [7], [8]. As a result, it is particularly difficult for glass tube makers to reduce the tube size for portable or handheld applications. Additionally, the mechanical and thermal properties of the tube envelope become especially important, as problems associated with bonding and heat storage start to arise when the size of the tube decreases [9].

In high-voltage applications such as dental imaging, the reduction in the tube size is even more challenging. In dental applications, for example, tube voltages in the range of 60–70 kV are required to generate X-rays with photon energy that is large enough to penetrate teeth, which are one of the hardest materials in a human body [10]–[13]. Application of such high voltages may cause charge to build up on the inner surface of the glass tube due to scattered electrons. As this built-up charge can deflect the electron beam near the anode, a distance of at least 5 mm is required between the glass tube and the anode to prevent that from happening [7], [8]. This imposes further restriction on the minimum diameter achievable with glass tubes for dental imaging.

In this study, we investigate the use of a ceramic envelope instead of the conventionally used glass to reduce the size

of the X-ray tube for dental imaging. Ceramic-to-metal seals have several properties that allow for a more robust, durable hermetic seal, and better electrical insulation than glass-to-metal seals [14], [15]. Professionally designed ceramic-to-metal seals can maintain hermeticity in a variety of harsh conditions, such as high- and low-temperature, corrosive, high-pressure, and high-vacuum environments [16]–[18]. Furthermore, the use of ceramic instead of glass enables to seal the X-ray tube by brazing, which supports higher temperature and throughput than conventional welding.

The initial use of ceramic tubes was reported by Hartl *et al.* [6], [7] in the early 80s, where they achieved a 25% reduction in the size of their industrial purpose X-ray system for nondestructive testing. In recent years, the use of ceramic has increased among X-ray tube makers using carbon nanotube (CNT) emitters [19], [20]. For CNT-based X-ray tubes, the high vacuum maintained by the use of ceramic envelopes is especially important as CNTs get easily oxidized at high voltages. However, comparisons between the performances of ceramic and glass tubes are lacking in these reports. In this study, we perform a direct comparison of a ceramic X-ray tube and a commercially available glass X-ray tube to fully understand the benefits of using ceramic envelopes in dental imaging.

By replacing glass with ceramic, a 43% reduction in X-ray tube size is achieved in this study. The current–voltage (I–V) characteristics of the glass and ceramic X-ray tubes are compared, and the latter is found to outperform the former despite the reduction in size. Furthermore, similar X-ray images of human teeth are obtained for the glass tube and the ceramic tube, as well as better limiting spatial resolution for the latter (7 versus 8 lines per mm), verifying the potential of using ceramic envelopes and the brazing process in mass-producing robust X-ray tubes for portable dental imaging.

II. Experiments

Fig. 1 shows a step-by-step fabrication process flow of the X-ray tube investigated herein. The target (anode) [Fig. 1(a)], which is made of a tungsten (W) and copper (Cu) alloy (W:Cu = 7:3), is attached to a kovar (nickel–cobalt ferrous alloy) supporter and a ceramic (93% Al_2O_3) body via brazing with a AgCu filler at 800 °C–850 °C in high vacuum ($<10^{-7}$ Torr) [Fig. 1(b)]. The anode target angle is 12.5 °C and the tungsten filament (cathode), which is 8.6 mm ± 0.3 mm in length, has 23 turns and an impedance value of 93.5 mΩ ± 30 mΩ [Fig. 1(c)]. For the glass tube (not shown), the anode target angle is also 12.5 °C and the tungsten filament is approximately 5.4 mm in length and has 14 turns and a cold resistance value of 145 mΩ ± 5 mΩ. The rim of the ceramic tube is covered by Mo–Mn metallization with nickel platting for hermetical sealing between the ceramic envelop and the kovar focuser [Fig. 1(c)–(f)].

Simulation of the electron trajectory with CST Charged Particle Studio Suite is used to optimize the tube design before fabrication. For stable performance, the filament undergoes an aging process before brazing. The aging process is achieved by repeatedly biasing the filament and the anode

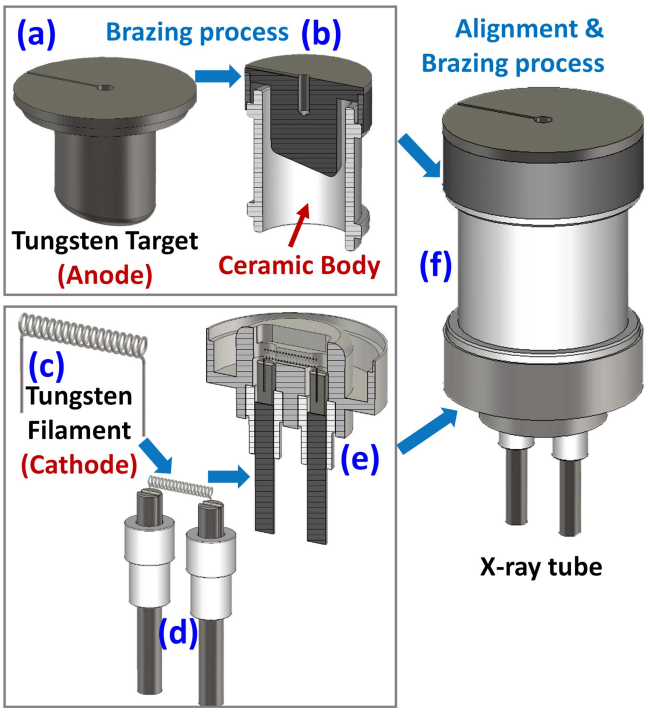

Fig. 1. Fabrication process of an X-ray tube with a ceramic vacuum seal. (a) Tungsten target. (b) Target attached to a ceramic body and a kovar supporter. (c) Tungsten filament. (d) Filament attached to electrodes. (e) Attachment of a kovar focuser to the filament. (f) Finished X-ray tube.

in an open-type high-vacuum chamber (10^{-7} Torr) to outgas the filament and anode as well as evaporate any native oxides.

To measure the I–V characteristics of the glass and ceramic X-ray tubes, the anode and the filament are connected to the Spellman high-voltage source S60 and Agilent dc voltage source E3632a, respectively. The measurement is performed in the worst possible case scenario to check the robustness of both the tubes. This is achieved by holding the anode voltage at 5 kV, while sweeping the filament voltage from 1 to 5 V until the anode current reaches 6 mA. Following this, 100 consecutive I–V cycles are performed under the same conditions to investigate the robustness of the tubes.

Anode voltage of 50 kV with 2 mA anode current and exposure time of 0.4 s are used to generate X-ray images of a human teeth phantom; 50 V instead of 60 or 70 kV is used for the laboratory setup as the specimen is placed near (25 cm) the X-ray tube and there is no additional filtration. X-ray dose measurements are performed by placing an RTI Black Piranha Dosimeter 25 mm from the X-ray tubes, while applying 70 kV to the anode and having 2 mA of anode current. The resolutions of the X-ray tubes are estimated by taking images of a line pair (LP) phantom. An exposure time of 0.4 s (with 35 kV, 4.5 mA) is used, and the LP phantom is placed right above the X-ray detector, while keeping the source-to-detector distance at 25 cm.

III. Results and Discussions

Fig. 2(a)–(c) shows, respectively, the side, front, and top (anode end) views of the simulated electron trajectories. The parameters used in the simulation are summarized in Table I.

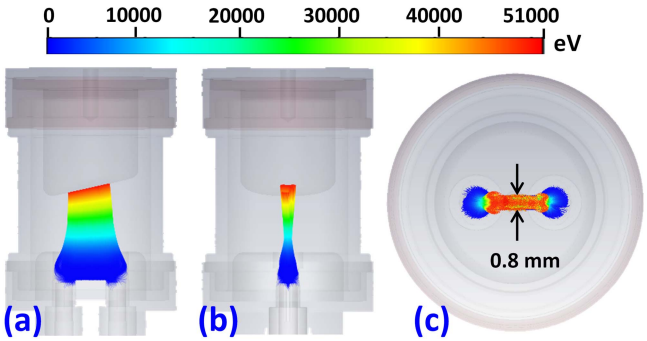

Fig. 2. Simulation of the electron trajectory with CST Charged Particle Studio Suite. (a) Front view. (b) Side view. (c) Top view of the actual focal spot size on the anode.

TABLE I
CST CHARGED PARTICLE STUDIO SUITE SIMULATION PARAMETERS

Parameter	Value
Emitting (Filament) Potential	4.5 V
Emission Distance	0.02 mm
Kinetic Value	5 eV
Focusing Cup Size (mm)	12(L) × 4.8(W) × 2.5(H)
Target Potential	70 kV
Kinetic Speed	5%
Filament Work function	4.54 eV
Anode-to-Filament Distance	11.44 mm

Anode Material: Tungsten
Filament Material: Tungsten

From the top view [Fig. 2(c)], an actual focal spot size (length) of 0.8 mm is estimated for the tube. Experimentally, the effective focal spot size (length) is estimated to be approximately 0.4 mm, which is compatible with dental applications [10]. The effective focal spot size of an X-ray tube depends on the anode angle (β) such that the effective focal spot size = actual focal spot size × sin(β) [21]. However, the simulated actual focal spot size of 0.8 mm corresponds to an effective focal spot size of 0.16 mm for an anode angle of 12.5°, which is different from the experimental value of 0.4 mm. The discrepancy is often due to the space charge effect caused by the electron cloud around the focusing cup, which can deviate electrons from their original path and thereby increase the effective focal spot size [22].

Fig. 3(a) and (b), respectively, shows the optical images of the ceramic-sealed X-ray tube developed in this study and a glass-sealed (Canon D-045) X-ray tube that is commonly used in handheld dental X-ray imaging systems. The length and diameter of the ceramic-sealed X-ray tube proposed herein are, respectively, 56 and 27 mm. The dimensions of the glass X-ray tube are 75 and 31 mm, respectively, making the ceramic-sealed X-ray tube approximately 43% smaller than the glass-sealed X-ray tube in volume.

It should be noted that smaller glass tubes (e.g., 17 mm × 17 mm, Sunje) have been developed [23] but these cannot be applied in dental imaging as they are only capable of low-voltage (11 kV) applications. In the case of ceramic tubes,

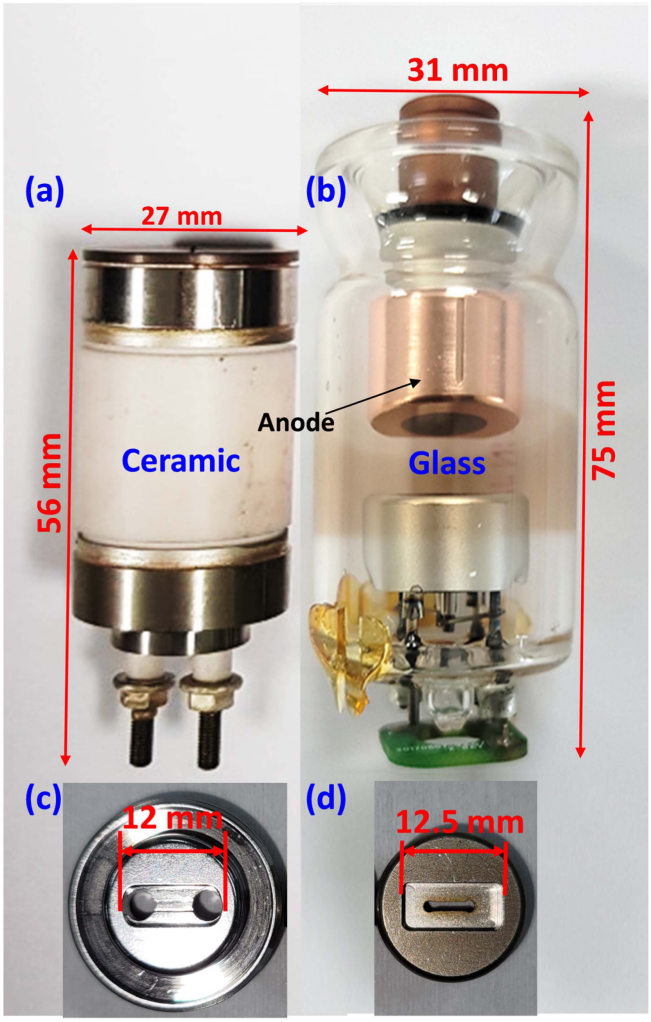

Fig. 3. Optical images of the dental X-ray tubes used in this study. (a) Ceramic tube developed herein. (b) Commercial glass X-ray tube (Canon D-045). (c) Focusing cup of the ceramic tube (focuser depth = 2.5 mm). (d) Focusing cup of the glass tube (focuser depth = 3.8 mm).

the smallest in the market is Xoft Inc., 50 kV miniature (10 mm × 2.25 mm) [24], [25]. The exceedingly small diameter (2.25 mm) of this ceramic tube underscores the high electrical insulation of the ceramic envelope. Fig. 3(c) and (d) shows the optical images of the focusing cups of the ceramic and glass sealed X-ray tubes, respectively. Relative to the size of the filament, the focusing cup of the glass tube is much wider and longer than that of the ceramic tube. Among other factors, which include the filament to anode distance, the smaller focusing cup size of the ceramic tube could be the reason why the effective focal spot size of the ceramic tube is smaller than that of the glass tube.

Despite being smaller than the glass-sealed, the ceramic-sealed X-ray tube shows better tube (anode) current stability during 100 consecutive I–V measurements (Fig. 4). The anode current of the glass X-ray tube degraded by 5.21% during the 100 consecutive measurements, whereas that of the ceramic-sealed X-ray tube decreased by only 0.01%. The better performance and stability exhibited by the ceramic-

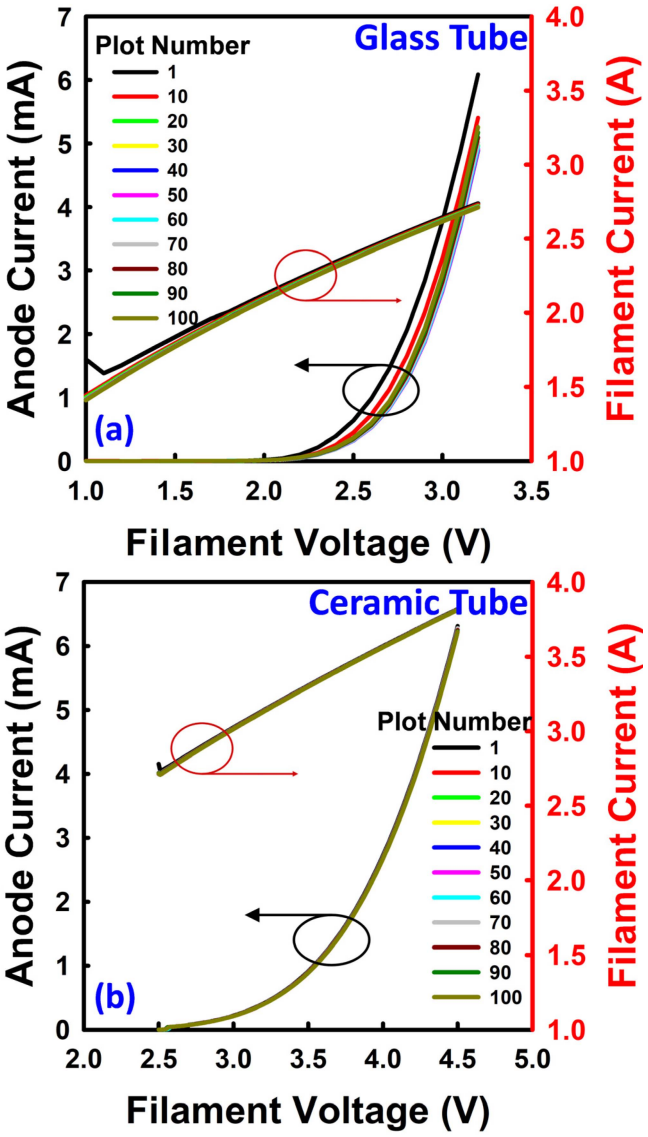

Fig. 4. Consecutive current–voltage (*I–V*) characteristics of (a) glass and (b) ceramic X-ray tubes. 100 consecutive *I–V* characteristics were measured, and for clarity, only the 1st, 10th, 20th, and so on (as indicated by the *Plot Number*) are shown. The anode voltage was 5 kV for all measurements.

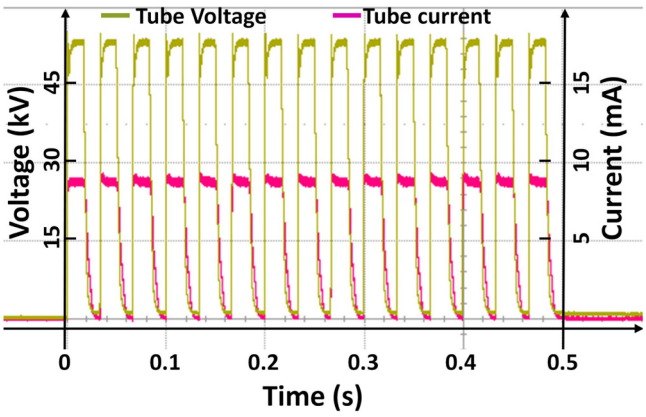

Fig. 5. Waveforms of the current–voltage characteristics of the ceramic X-ray tube. The frequency was 30 Hz, and the duty cycle was 50%.

sealed X-ray tube are attributed to a damage-free brazing process.

Maintaining high vacuum inside the tube is crucial for high and stable current. Compared with the conventional glass-to-metal welding, ceramic-to-metal brazing supports hermetical sealing at higher temperature and thereby achieves higher vacuum [14]–[18]. This significantly reduces oxidation of components inside the ceramic X-ray tubes and leads to a decrease in the outgassing phenomena and arcing during the emission of electrons at high voltages.

The lower turn-on voltage exhibited by the glass-sealed X-ray tube compared with the ceramic-sealed tube is related to the smaller filament size of the former, which translates to a lower resistance value. To protect the anode from melting under constant bias, it is desirable to operate the tube with pulsed anode voltage. The 50 kV anode voltage pulses with a frequency of 30 Hz yielded stable tube current of 9 mA (Fig. 5), indicating good response to input pulses for the ceramic-sealed X-ray tube.

Using the ceramic and glass-sealed X-ray tubes, X-ray images were generated for a specimen of human teeth (Fig. 6). Interestingly, the X-ray images generated by the two tubes show no significant difference in resolution, despite the size differences. The resolutions of the ceramic and glass sealed X-ray tubes are estimated by taking images of an LP phantom [Fig. 7(a) and (b)]. An LP phantom consists of a thin foil of lead sandwiched between plastic plates. Linear slits with a range of widths are cut in the foil. The slits alternate with linear bars of the foil of equal width, and one slit and one bar are referred to as an LP. The numbers on the left side of the LP phantom images shown in Fig. 7(a) and (b) specify the number of LPs per millimeter (LP/mm). Limiting spatial resolutions of approximately 8 and 7 LP/mm are estimated for the ceramic- and glass-sealed X-ray tubes, respectively, [Fig. 7(c)]. Although the ceramic tube has a longer filament than the glass tube, the higher limiting spatial resolution may be due to combinational effects of the shape of the focusing cup and the filament-to-anode distance on the electron trajectories, as explained earlier.

As the envelopes for both the ceramic and glass tubes are different, the actual dose under the same conditions could be different due to the differences in the attenuation characteristics of ceramic and glass. Fig. 8 shows the radiation dose comparison of both X-ray tubes during 1 s with 70 kV (tube current of 2 mA). The results show that the ceramic X-ray tube has an inherent (total) filter equivalent to 1.7 mm aluminum (Al), whereas that of the glass tube is 1.2 mm Al [according to IEC 60601-1-3 (IEC 2008)]. Because of this, the ceramic tube produces an average of 1.6 mGy/s of dose, which is slightly lower than the 2 mGy/s produced by the glass tube under the same operating conditions. This is a drawback for ceramic-sealed X-ray tubes and the effects may include poor image brightness [compare Fig. 4(b) and (c)]. However, for handheld dental imaging systems, a total filter of 2 mm Al is required [10]. This implies that during the assembly of a dental

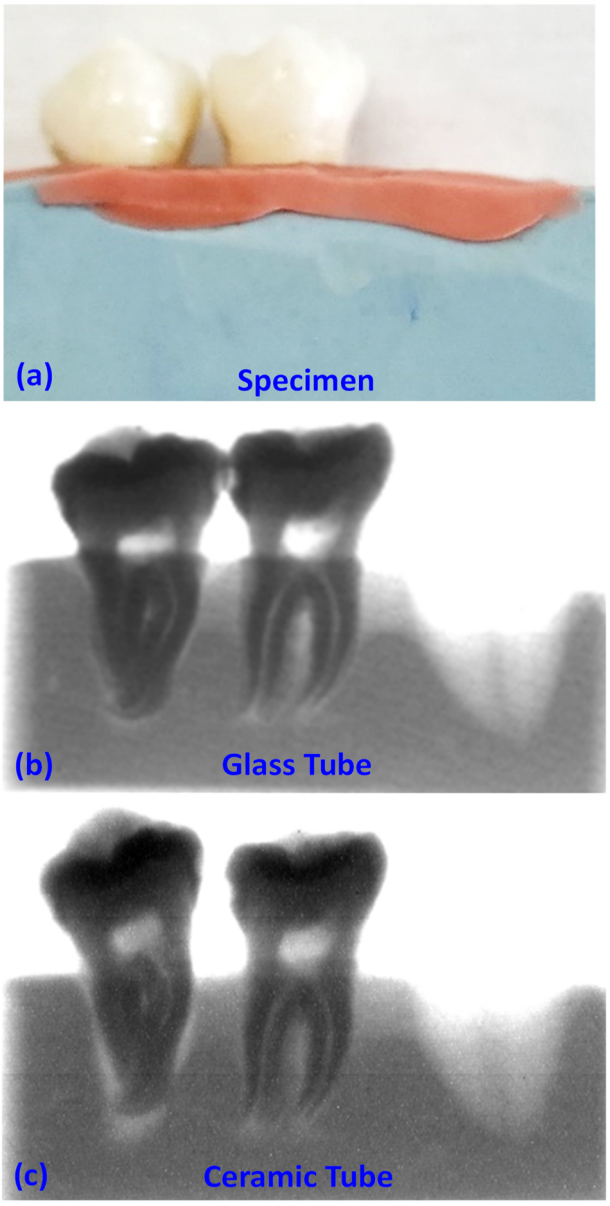

Fig. 6. X-ray images of a human teeth phantom taken using the ceramic and glass X-ray tubes. (a) Specimen. (b) Image of the ceramic tube. (c) Image of the glass tube. Anode voltage of 50 kV, anode current of 2 mA, and exposure time of 0.4 s were used to generate the X-ray images.

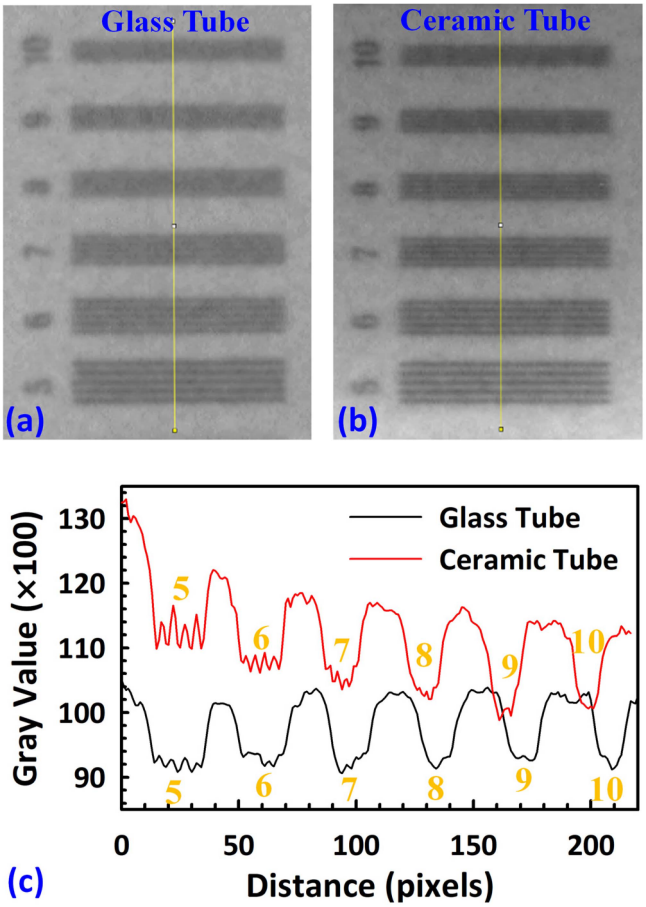

Fig. 7. Limiting spatial resolution calculation using a plot profile of X-ray images of an LP phantom. (a) Image taken by the glass tube. (b) Image taken by the ceramic tube. (c) Line profiles of the gray values. The numbers on the left side of the images in (a) and (b) specify the number of LPs per mm (LP/mm). The same numbers are shown in (c).

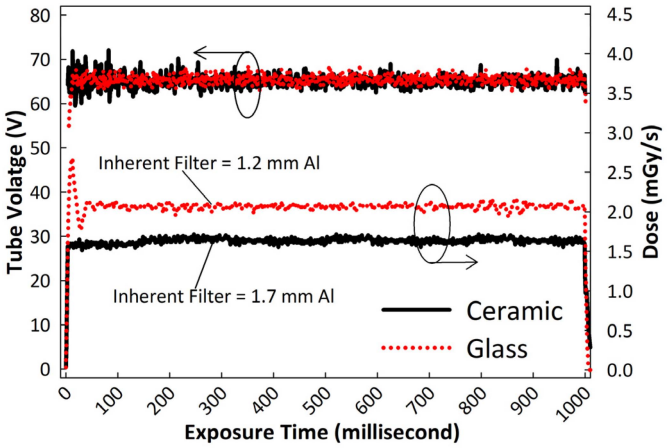

Fig. 8. Radiation doses of the glass and ceramic X-ray tubes.

X-ray system, comparatively thicker filters must be added for glass than ceramic tubes.

The above results show that the reduction in size does not affect the performance of the X-ray tube. As size reduction is important for portable medical imaging and handheld dental applications, the ceramic-sealed X-ray tube presented herein paves the way for such applications. There are several other advantages to using ceramic instead of glass as the X-ray tube cover. Ceramic-to-metal fusing can be achieved via brazing, which is more convenient for mass production than welding. Mass production will effectively reduce fabrication costs and processing time. Additionally, brazing can be performed at higher temperature than welding, which is desirable for better hermetical sealing. Moreover, ceramic-sealed X-ray tubes have a longer tube life than glass-sealed X-ray tubes due to the detrimental effects of tungsten deposits, which can easily accumulate on glass than ceramic during operation [26]. Furthermore, the dielectric constant of ceramic is higher than that of glass, enabling higher vacuum and process tolerance.

IV. Conclusion

We have demonstrated a ceramic-based X-ray tube that is smaller and more robust than a glass X-ray tube used in dental imaging. The ceramic tube is produced by brazing, which is desirable for mass production compared with welding. Using CST Charged Particle Studio Suite, we achieved an optimized actual focal spot size of 0.8 mm. The ceramic X-ray tube demonstrated herein was able to resolve 8 LPs/mm at 35 kV and with a tube current of 4.5 mA. Because of the ceramic envelope and the damage-free brazing process, we achieved superior I–V characteristics and higher stability of the filament, without compromising tube resolution, as seen in the high-resolution X-ray images of a human teeth phantom taken by the ceramic X-ray tube. These results verify the potential of using ceramic envelopes in dental imaging to reduce the size and improve the robustness of X-ray tubes, as well as the use of brazing for their mass production.

References

[1] R. F. Mould, *A Century of X-rays and Radioactivity in Medicine*. Boca Raton, FL, USA: CRC Press, 2018.

[2] F. E. Zink, "X-ray tubes," *Radio Graph.*, vol. 17, no. 5, pp. 1259–1268, Sep. 1997, doi: 10.1148/radiographics.17.5.9308113.

[3] M. E. Herniter and W. D. Getty, "Thermionic cathode electron gun for high current densities," *IEEE Trans. Plasma Sci.*, vol. PS-15, no. 4, pp. 351–360, Aug. 1987, doi: 10.1109/TPS.1987.4316719.

[4] R. Jacobs, D. Morgan, and J. Booske, "Work function and surface stability of tungsten-based thermionic electron emission cathodes," *APL Mater.*, vol. 5, no. 11, Nov. 2017, Art. no. 116105, doi: 10.1063/1.5006029.

[5] N. C. Beese, "The focusing of electrons in an X-ray tube," *Rev. Sci. Instrum.*, vol. 8, no. 7, pp. 258–262, Jul. 1937, doi: 10.1063/1.1752305.

[6] W. Hartl, D. Peter, and K. Reiber, "A metal/ceramic diagnostié X-ray tube," *Philips Tech. Rev.*, vol. 41, no. 4, pp. 126–134, Feb. 1983.

[7] W. Hartl, D. Peter, and K. Reiber, "Metal/ceramic X-ray tubes for nondestructive testing," *Philips Tech. Rev.*, vol. 41, no. 1, pp. 24–29, 1983.

[8] R. Behling, *Modern Diagnostic X-Ray Sources*. Boca Raton, FL, USA: CRC Press, 2015.

[9] R. Behling, "X-ray sources: 125 years of developments of this intriguing technology," *Phys. Medica*, vol. 79, pp. 162–187, Nov. 2020, doi: 10.1016/j.ejmp.2020.07.021.

[10] A. D. Gulson and J. R. Holroyd, "Guidance on the safe use of hand-held dental X-ray equipment," Public Health England, London, U.K., Tech. Rep. PHE-CRCE-023, Feb. 2016.

[11] T. J. McGiff, R. A. Danforth, and E. E. Herschaft, "Maintaining radiation exposures as low as reasonably achievable (ALARA) for dental personnel operating portable hand-held X-ray equipment," *Health Phys.*, vol. 103, no. 2, pp. S179–S185, Aug. 2012, doi: 10.1097/HP.0b013e318259fa29.

[12] S. Hong *et al.*, "Development and evaluation of a CMOS sensor-based digital intra-oral radiographic system," *IEEE Trans. Nucl. Sci.*, vol. 52, no. 1, pp. 256–261, Feb. 2005, doi: 10.1109/TNS.2004.843167.

[13] W. E. R. Berkhout, A. Suomalainen, D. Brüllmann, R. Jacobs, K. Horner, and H. C. Stamatakis, "Justification and good practice in using handheld portable dental X-ray equipment: A position paper prepared by the European Academy of DentoMaxilloFacial Radiology (EADMFR)," *Dentomaxillofacial Radiol.*, vol. 44, no. 6, pp. 1–6, Jul. 2015, doi: 10.1259/dmfr.20140343.

[14] R. W. Davidge and A. G. Evans, "The strength of ceramics," *Mater. Sci. Eng.*, vol. 6, no. 5, pp. 281–298, Nov. 1970, doi: 10.1016/0025-5416(70)90064-9.

[15] S. Mishra, A. Sharma, D. H. Jung, and J. P. Jung, "Recent advances in active metal brazing of ceramics and process," *Metals Mater. Int.*, vol. 26, no. 8, pp. 1087–1098, Nov. 2019, doi: 10.1007/s12540-019-00536-4.

[16] W. H. Kohl, "Ceramics and ceramic-to-metal sealing," *Vacuum*, vol. 14, no. 9, pp. 333–354, Sep. 1964, doi: 10.1016/0042-207X(64)90129-0.

[17] S. S. Cole and G. Sommer, "Glass-migration mechanism of ceramic-to-metal seal adherence," *J. Amer. Ceram. Soc.*, vol. 44, no. 6, pp. 265–271, Jun. 1961, doi: 10.1111/j.1151-2916.1961.tb15376.x.

[18] N. Deng, J. Zhao, L. Yang, and Z. Zheng, "Effects of brazing technology on hermeticity of alumina ceramic-metal joint used in nuclear power plants," *Frontiers Mater.*, vol. 7, pp. 377–384, Feb. 2021, doi: 10.3389/fmats.2020.580938.

[19] J.-W. Jeong, J.-W. Kim, J.-T. Kang, S. Choi, S. Ahn, and Y.-H. Song, "A vacuum-sealed compact X-ray tube based on focused carbon nanotube field-emission electrons," *Nanotechnology*, vol. 24, no. 8, Mar. 2013, Art. no. 085201, doi: 10.1088/0957-4484/24/8/085201.

[20] J.-W. Jeong, J.-T. Kang, S. Choi, J.-W. Kim, S. Ahn, and Y.-H. Song, "A digital miniature X-ray tube with a high-density triode carbon nanotube field emitter," *Appl. Phys. Lett.*, vol. 102, no. 2, Jan. 2013, Art. no. 023504, doi: 10.1063/1.4776222.

[21] R. T. Bergeron, "Manufacturers' designation of diagnostic X-ray tube focal spot size: A time for candor," *Radiology*, vol. 111, no. 2, pp. 487–488, May 1974, doi: 10.1148/111.2.487.

[22] M. Ferrario, M. Migliorati, and L. Palumbo, "Space charge effects," in *Proc. CAS-CERN Accel. School, Adv. Accel. Phys.*, Aug. 2013, pp. 331–356, doi: 10.5170/CERN-2014-009.331.

[23] Sunje Inc, Busan, South Korea. X-ray Tube Leaflet. Accessed: May 24, 2021. [Online]. Available: http://sunstat.com/en/x-ray-tube-leaflet/

[24] M. J. Rivard, S. D. Davis, L. A. DeWerd, T. W. Rusch, and S. Axelrod, "Calculated and measured brachytherapy dosimetry parameters in water for the Xoft Axxent X-ray Source: An electronic brachytherapy source a," *Med. Phys.*, vol. 33, no. 11, pp. 4020–4032, Oct. 2006, doi: 10.1118/1.2357021.

[25] Xoft Inc, San Jose, CA, USA. X-ray Source. Accessed: May 24, 2021. [Online]. Available: https://www.xoftinc.com/assets/mc466_x-ray_source_revb.pdf

[26] Spellman High Voltage Electronics Corporation, Hauppauge, NY, USA. Common X-ray Tube Failure Modes. Accessed: May 24, 2021. [Online]. Available: https://www.spellmanhv.com/ko/Technical-Resources/Application-Notes-X-Ray-Generators/AN-02